1986AJ.....92.1238P



# PROBES OF LARGE-SCALE STRUCTURE IN THE CORONA BOREALIS REGION[a]

M. POSTMAN
Princeton University Observatory, Peyton Hall, Princeton, New Jersey 08544

J. P. HUCHRA,[b] AND M. J. GELLER
Harvard-Smithsonian Center for Astrophysics, 60 Garden Street, Cambridge, Massachusetts 02138

*Received 8 July 1986; revised 15 August 1986*

## ABSTRACT

We discuss a redshift survey of the Corona Borealis region. Our unfilled deep survey consists of five probes complete to $m_R = 15.7$. These cover 3.4 square degrees distributed over a $\sim 16.4$ square degree region. We include redshifts, magnitudes, and positions for the 83 galaxies in this survey. A complementary filled survey covers 39.2 square degrees and is complete to $m_{B(0)} = 15.5$. There are 37 galaxies in this survey, which is part of the CfA redshift extension (de Lapparent, Geller, and Huchra 1986). The combined survey provides further support for the "bubble-like" geometry revealed by the shallower CfA survey. The redshift distribution for the new survey is remarkably similar to the distribution in the neighboring Boötes region. We detect a void near Boötes with a radius $\gtrsim 13h^{-1}$ Mpc ($H_0 = 100h$ km s$^{-1}$ Mpc$^{-1}$). This survey also indicates that the structure of voids and surfaces in the galaxy distribution is insensitive to luminosity for $M_{B(0)} \lesssim -17.4$.

## I. INTRODUCTION

Complete redshift surveys which map out the large-scale structure of the universe are important for testing the predictions of galaxy- and cluster-formation models (Einasto *et al.* 1980; Tarenghi *et al.* 1980; Gregory *et al.* 1981; Binggeli 1982; de Lapparent, Geller, and Huchra 1986). These surveys also provide the basis for estimating the universal mean mass density (Sargent and Turner 1977; Davis and Peebles 1983), and for measuring large-scale peculiar velocity flows (Aaronson *et al.* 1982; Faber 1986).

Redshift surveys of large volumes of the universe generally fall into two broad categories: (1) *filled surveys*, which cover a large continuous area on the sky, and (2) *unfilled surveys*, which cover several areas well separated on the sky. The CfA redshift survey (Huchra *et al.* 1982) and its extension (de Lapparent, Geller, and Huchra 1986, LGH) fall in the first category; the probes of the void in Boötes (Kirshner, Oemler, Schechter, and Shectman 1981, 1986, KOSS) fall in the second.

Filled surveys tend to be shallower than unfilled ones covering comparable (or even larger) volumes because of the limited availability of time on large telescopes. In unfilled surveys, the detection of large structures is limited by the ratio of the area actually sampled to the total area spanned by the set of probes. The discovery of the void in Boötes demonstrates that unfilled surveys provide an efficient method for identifying large structures. In contrast, the CfA survey demonstrates the importance of filled surveys for understanding the precise topology of the galaxy distribution.

In this paper, we combine a deep, unfilled survey of the large-scale structure and galaxy distribution in the Corona Borealis region (hereafter referred to as Cor Bor) with a filled survey of the foreground structure. The filled survey is complete to $m_{B(0)} = 15.5$ over an area of 39.2 square degrees and is part of the CfA redshift survey, which reveals the "bubble-like" structure of the large-scale galaxy distribution (LGH 1986). Part of a large void and a portion of the surrounding surface are included in the 39.2 square-degree survey. The deeper probes serve to set limits on the distribution of faint galaxies in this void and to examine the relative distribution of bright and faint galaxies in the surrounding surface.

The unfilled survey alone samples the galaxy distribution more directly associated with the Cor Bor supercluster (the six rich Abell clusters A2061, A2065, A2067, A2079, A2089, and A2092) at a redshift of $\sim 21\,000$ km s$^{-1}$. It reveals a void centered at 13 500 km s$^{-1}$ with a diameter of at least $26h^{-1}$ Mpc ($H_0 = 100h$ km s$^{-1}$ Mpc$^{-1}$). This void is in the same velocity range as the adjacent void in Boötes.

In fact, the velocity distribution in the Cor Bor survey is remarkably similar to the one for the nearby independent survey of Boötes (KOSS 1981, 1986). Together, the Boötes survey and the Cor Bor survey cover about 850 square degrees on the sky. The similarity of the redshift distributions provides further support for the picture suggested by LGH and underscores the common occurrence of large voids in the galaxy distribution.

Sections II and III describe the photometric, astrometric, and redshift data acquired for the Cor Bor study. Section IV contains the analysis and results. The conclusions are in Sec. V. Analysis of the dynamical and photometric properties of the Cor Bor supercluster will be published in later papers.

## II. PHOTOMETRY AND ASTROMETRY

We have acquired photographic $R$ photometry calibrated with CCD images for galaxies in an $\sim 7.9$ square-degree area in the Cor Bor region (see Fig. 3). The photometric data are required to estimate the completeness of the redshift survey and to study the luminosity dependence of the galaxy distribution.

We mapped the Cor Bor region by digitizing sections of glass copies of Palomar Observatory Sky Survey (POSS) plates E-121 and E-1092 with the PDS microdensitometer at the Kitt Peak National Observatory. Each section measures $4 \times 4$ cm ($\sim 45' \times 45'$). We scanned a total of 14 sections with a nonoverlapping $20 \times 20\,\mu$m aperture ($1.35'' \times 1.35''$) at a scan speed of 39 mm s$^{-1}$. Each section is then an array of $2000 \times 2000$ 12-bit pixels.

[a] Work reported here based on observations obtained at the Multiple Mirror Telescope—a joint facility of the Smithsonian Institution and the University of Arizona.

[b] Visiting Scientist, NOAO.

 0004-6256/86/061238-10$00.90 © 1986 Am. Astron. Soc. 

© American Astronomical Society • Provided by the NASA Astrophysics Data System

1986AJ.....92.1238P



### *a) Star-Galaxy Classification*

We use the star-galaxy-plate flaw-classification algorithm developed by Kurtz *et al.* (1985; see reference for details). In this procedure, we first sky subtract the digitized image, then identify "objects" as all sets of pixels above a limiting isophote which are connected to the positions of local maxima. The values of the second and third moments from the density-weighted centroid, the isophotal count rate, the number of local maxima in the object, and the central-density to total-density ratio determine whether an object is classified as a star, galaxy, multiple object (e.g., star + galaxy), or noise. The algorithm is not fully automated and human intervention is required for approximately one-third of the objects bright enough to classify.

The object-finding routine yields catalogs which are complete to $m_R = 20$ (Kurtz *et al.* 1985). The object-classification routine is $\gtrsim 95\%$ accurate to $m_R = 16$ and $\sim 90\%$ accurate to $m_R = 18.5$. The Kurtz software identifies all the Zwicky galaxies located in the PDS survey regions. Provided they were bright enough to classify, all galaxies identified by eye from CCD images of this region were also identified as galaxies by the star/galaxy separation algorithm. As a final check of the reliability of this algorithm, the A2079 field was digitized at the Yale PDS facility, using a different copy of POSS plate E-1092, and the image was reduced using FOCAS (Valdes 1982) software. The galaxy tables for the YALE/FOCAS and KPNO/KURTZ images are identical to $m_R = 15.9$. A probable flaw on POSS plate E-1092 is located at $\alpha = 15^h18^m14.5^s$, $\delta = +30°32'33''$.

### *b) Magnitude Calibration*

CCD measurements of galaxies in the Cor Bor region yield a transformation from isophotal and aperture PDS counts to magnitudes. $F$ band exposures of A2061, A2067, A2079, A2089, and A2092 were obtained using the CCD camera on the Mount Hopkins 61 cm telescope. The $F$ filter data are transformed to magnitudes in Kron-Cousins $R$ (Kron *et al.* 1953) assuming a $(V-R)_{KC}$ color of 0.6 for each object. The transformation is not very sensitive to color (Schild and Kent 1981). The CCD magnitudes are calibrated by comparison with observations of M67 (Schild 1984). We estimate that the external zero-point error is $\leqslant 0.03$ mag.

The PDS calibration is obtained by comparing CCD magnitudes for isolated galaxies brighter than $m_R = 18.2$ with the PDS counts within a synthetic aperture. The same aperture size (21.6″) is used for both the CCD and PDS data. The PDS-to-$R_{KC}$ calibration constants for POSS plates E-121 and E-1092 differ by $\sim 0.5$ mag (using the KPNO PDS images). The variation in the calibration constant between two points on the same plate, however, is $\lesssim 0.05$ mag. Figure 1 shows the deviation from the mean calibration constant as a function of CCD magnitude for the 56 galaxies used as calibrators. The scatter is 0.16 mag and the deviations are independent of magnitude out to $m_R = 18.2$.

Any galaxy with aperture and isophotal magnitudes differing by more than 0.25 mag is examined in detail. All such galaxies have nearby companions and many were tagged as multiple objects during the classification stage.

### *c) Equatorial Coordinates*

The positions of $\sim 20$ SAO stars in the vicinity of each digitized section of the POSS E plates were recorded on the CfA measuring engine. A calculation of the local aspect solution yields the equatorial coordinates (1950.0) of $\sim 12$ PDS objects identified as stars in each section. A new aspect solution computed for these 12 stars is then used to determine the equatorial coordinates of all the PDS objects in the section. The equatorial coordinates are accurate to $\sim 2''$.

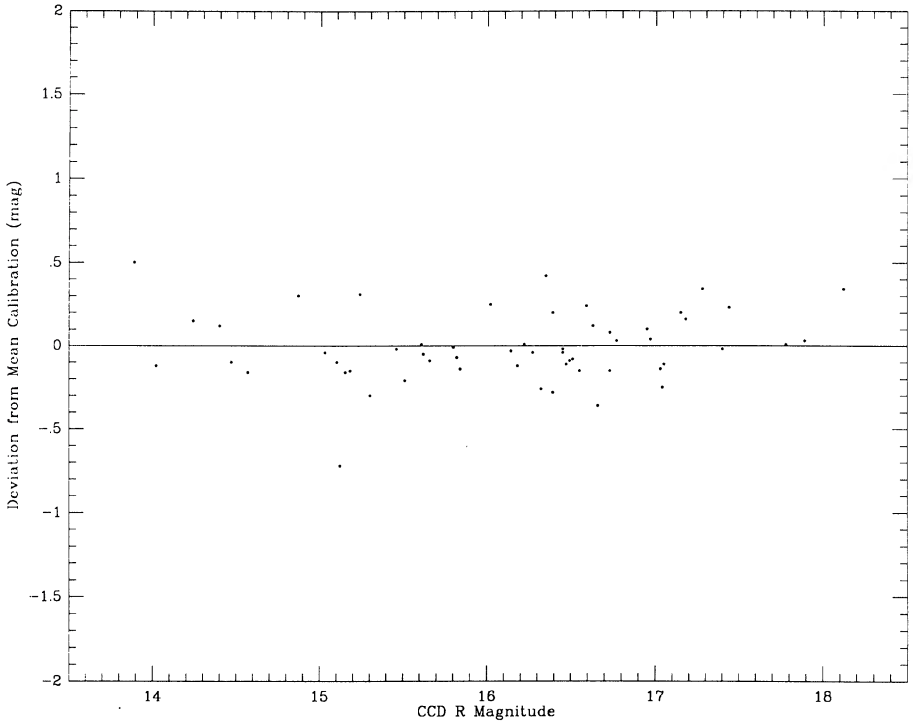


FIG. 1. Deviation from the mean PDS-to-$R_{KC}$ calibration constant as a function of $R_{KC}$ magnitude for the 56 galaxies used as calibrators.

© American Astronomical Society • Provided by the NASA Astrophysics Data System

1986AJ.....92.1238P



SURVEY FIELDS IN BOÖTES AND CORONA BOREALIS

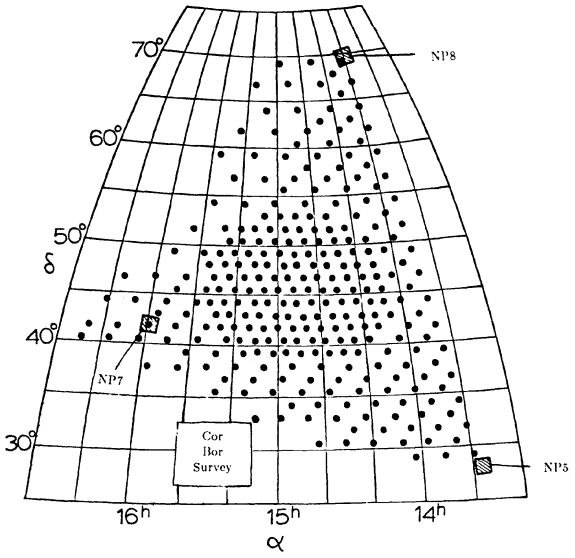


FIG. 2. Location on the sky of the Cor Bor survey and the original Boötes survey fields NP 5, NP 7, and NP 8 (KOSS 1981). The small circles show the location of the fields in a recent more detailed survey of Boötes (after KOSS 1986).

## III. SPECTROSCOPIC OBSERVATIONS AND SURVEY PROPERTIES

We have measured 120 redshifts for galaxies in the region

$$15.2^{h} \leqslant \alpha \leqslant 15.7^{h},$$
$$26.5\,^{\circ} \leqslant \delta \leqslant 32.5\,^{\circ}, \qquad (1)$$

an area of $\sim 39.2$ square degrees. Of the 120 redshifts, 34 were obtained at the 1.5 m telescope at Mount Hopkins Observatory using the Varo 8605/3603 image-intensifier package and photon-counting Reticon system. These galaxies are included in the extension of the CfA redshift survey to $m_{B(0)} = 15.5$ (LGH). The spectral coverage of the 1.5 m spectrograph is 4500–7100 Å at $\sim 5.1$ Å resolution. The typical uncertainty in the 1.5 m redshifts is $\sim 30$ km s$^{-1}$. Redshifts for three additional galaxies, also included in the extension of the CfA survey, were obtained from the literature (see velocity source list for Table II).

The remaining 83 redshifts were obtained using the photon-counting Reticon system at the Multiple Mirror Telescope (MMT). The MMT spectrograph was used to measure the redshifts of galaxies in the vicinity of the Abell clusters in Cor Bor. The MMT observations were made with a blue-sensitive tube covering the range 3400–7000 Å at $\sim 6.5$ Å resolution. The typical uncertainty in the MMT redshifts is $\sim 50$ km s$^{-1}$.

The combined sample we analyze is complete to $m_{B(0)} = 15.5$ over the entire survey region (1). Over an area of 3.4 square degrees included within region (1), the survey is complete to $m_R = 15.7$ (see fields enclosed by solid lines in Fig. 3). This unfilled $R$ magnitude limited survey of Cor Bor is spread over $\sim 16.4$ square degrees and fills 20% of this area. On average, there are 17 galaxies per field. For comparison, the KOSS (1986) survey of Boötes is spread over $\sim 750$ square degrees and fills 2% of the area. The KOSS probes were chosen so that each field would contain one to two galaxies brighter than $m_F \approx 16$. Figure 2 shows the location of the Boötes and Cor Bor survey fields on the sky.

Figure 3 shows the distribution on the sky of all galaxies brighter than $m_R = 18$ for the portions of the Cor Bor region where we have PDS $R$ photometry. A2069 is a background cluster at a redshift of 0.115. The circles indicate the centers of Abell clusters [from Abell (1958)], which are typically offset from the locations of galaxy surface-density maxima by only 3–5 arcmin ($\sim 250h^{-1}$ kpc). A2067 and A2079 have the largest offsets.

Dashed lines indicate the PDS survey limits. The solid lines in Fig. 3 are the boundaries of the complete redshift survey to $m_R = 15.7$. There are a total of 83 galaxies in this 3.4 square-degree survey. Note that the survey region centered at $15^{h}24^{m}$, $+23\,^{\circ}05'$ does not contain an Abell cluster.

Table I lists the galaxy ID (col. 1), 1950 coordinates (cols. 2 and 3), isophotal magnitude (col. 4), aperture magnitude (col. 5), aperture size (col. 6), object type (col. 7), and heliocentric velocity and velocity error (cols. 8 and 9) for the 83 galaxies in the unfilled survey. All galaxies originally classified as multiple objects are denoted by the G + symbol in column 7. Magnitudes for the G + objects correspond to the galaxian component only. Objects with an asterisk in column 5 have companions that lie within the aperture. In such cases, the isophotal magnitude provides a good approximation to the aperture magnitude.

Table II lists the galaxy ID (col. 1), 1950 coordinates (cols. 2 and 3), Zwicky $B(0)$ magnitude (col. 4), heliocentric velocity and velocity error (cols. 5 and 6), and velocity source (col. 7) for the 37 galaxies in the filled survey. Magnitudes in Tables I and II are not corrected for $K$ dimming or for galactic absorption.

## IV. ANALYSIS

### *a) the Radial-Velocity Distribution*

Figure 4(a) is a velocity histogram for the filled survey. The void in the 5000–10 000 km s$^{-1}$ range is the one discussed at length in LGH. The peak at 9500 km s$^{-1}$ is part of the thin surface which surrounds the void. Figure 4(b) shows the velocity histogram for the unfilled survey. Only one galaxy is added in the nearby void and the thin surface at 10 000 km s$^{-1}$ is apparent. The Cor Bor supercluster is responsible for the enormous peak and a void appears to separate Cor Bor from the foreground structure at 10 000 km s$^{-1}$. The curves in both figures show the redshift distribution expected for a uniform galaxy distribution with a galaxy luminosity function of the Schechter (1976) form

$$\Phi(L)dL = \phi^{*}\left(\frac{L}{L^{*}}\right)^{\alpha} \exp\left(-L/L^{*}\right) d\left(\frac{L}{L^{*}}\right). \qquad (2)$$

We use the values $M^{*}_{B(0)} = -19.40$, $\alpha = -1.3$, and $\phi^{*} = 0.0143h^{3}$ Mpc$^{-3}$ derived for the CfA redshift survey (Davis and Huchra 1982). We use the CfA values for the $R$ band as well, assuming $[B(0) - R] = 1.5$. A determination of $\phi^{*}$ based on data from our $R$ survey yields a value $\sim 2$ times larger than the CfA value. The difference is caused by the presence of the Cor Bor supercluster, which dominates the deep sample. Use of this higher value would lead to overestimation of the significance of voids in the survey. The CfA $\phi^{*}$ is thus the conservative choice in setting limits on the distribution of voids.

Analysis of the redshift distribution in the combined survey yields limits on the properties of the large-scale structure

© American Astronomical Society • Provided by the NASA Astrophysics Data System

1986AJ.....92.1238P



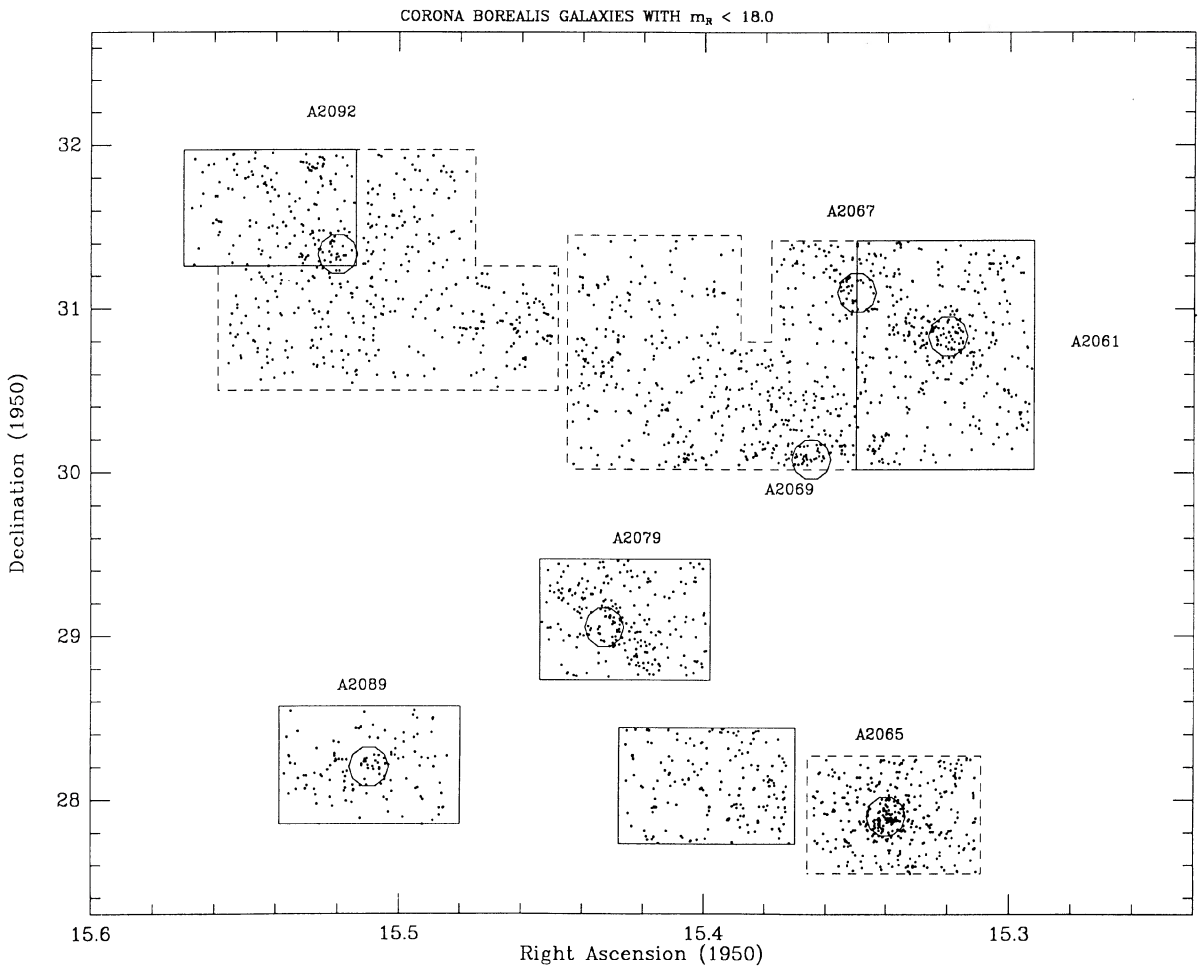


FIG. 3. Distribution on the sky of all galaxies ($N_{gal} = 2392$) brighter than $m_R = 18$ for the portions of the Cor Bor region where PDS photometry has been obtained. Large circles denote the centers of Abell clusters. Survey boundaries are denoted by dashed lines. Solid lines denote fields with complete redshift data.

TABLE I. Data for unfilled survey of the Cor Bor region.

| ID | R.A. (1950) | Dec. | $R_{iso}$ | $R_{ap}$ | Size (″) | Object type | Vel. | Err. |
|---|---|---|---|---|---|---|---|---|
| | | | | Abell 2061 North | | | | |
| 128 | 15:19:17.50 | 30:50:58.2 | 14.05 | * | 21.6 | G+ | 23706 | 34 |
| 139 | 15:19:09.29 | 30:50:13.6 | 14.53 | * | 21.6 | | 9350 | 28 |
| 71 | 15:19:59.47 | 31:24:40.9 | 14.60 | 14.74 | 21.6 | G+ | 9483 | 24 |
| 103 | 15:19:31.28 | 30:53:57.1 | 14.69 | 14.84 | 21.6 | | 23484 | 42 |
| 210 | 15:18:21.37 | 31:16:43.6 | 15.04 | 14.79 | 21.6 | G+ | 21921 | 35 |
| 54 | 15:20:09:30 | 31:24:14.6 | 15.27 | 15.32 | 21.6 | G+ | 34279 | 36 |
| 108 | 15:19:27.69 | 30:53:13.3 | 15.29 | 15.30 | 21.6 | | 24366 | 35 |
| 129 | 15:19:15.33 | 31:00:42.5 | 15.30 | 15.26 | 21.6 | | 22242 | 37 |
| 86 | 15:19:43.23 | 30:46:33.9 | 15.37 | 15.31 | 21.6 | | 23542 | 45 |
| 2 | 15:20:52.55 | 31:09:42.8 | 15.47 | 15.43 | 21.6 | | 24129 | 46 |
| 191 | 15:18:39.97 | 30:52:09.4 | 15.61 | 15.58 | 21.6 | | 23263 | 49 |
| 153 | 15:19:03.01 | 30:51:21.9 | 15.63 | 15.57 | 21.6 | | 9172 | 43 |
| 136 | 15:19:11.69 | 30:56:09.6 | 15.67 | 15.66 | 21.6 | | 26960 | 53 |
| | | | | Abell 2061 South | | | | |
| 92 | 15:19:07.90 | 30:45:46.0 | 14.32 | * | 21.6 | | 22746 | 37 |
| 94 | 15:19:05.06 | 30:45:09.2 | 14.94 | 15.09 | 21.6 | | 23711 | 35 |
| 96 | 15:18:58.92 | 30:45:06.4 | 15.07 | 15.08 | 21.6 | | 22888 | 35 |
| 108 | 15:18:50.46 | 30:34:19.1 | 15.16 | 15.20 | 21.6 | | 23538 | 41 |
| 86 | 15:19:10.87 | 30:42:06.0 | 15.18 | 15.26 | 21.6 | | 23241 | 47 |
| 128 | 15:18:34.66 | 30:39:02.9 | 15.22 | * | 21.6 | G+ | 9558 | 38 |
| 147 | 15:18:01.14 | 30:29:07.7 | 15.27 | 15.03 | 21.6 | G+ | 19914 | 37 |
| 154 | 15:17:47.96 | 30:22:00.7 | 15.28 | 15.32 | 21.6 | | 24717 | 52 |

© American Astronomical Society • Provided by the NASA Astrophysics Data System

1986AJ.....92.1238P



TABLE I. (continued)

| ID | R.A. (1950) | Dec. | $R_{iso}$ | $R_{ap}$ | Size (") | Object type | Vel. | Err. |
|---|---|---|---|---|---|---|---|---|
| | | | | Abell 2061 South | | | | |
| 157 | 15:17:45.95 | 30:22:06.9 | 15.32 | 15.33 | 21.6 | | 24289 | 45 |
| 54 | 15:19:56.04 | 30:35:09.9 | 15.32 | 15.37 | 21.6 | | 23206 | 37 |
| 141 | 15:18:05.56 | 30:30:02.2 | 15.34 | 15.30 | 21.6 | | 19846 | 30 |
| 133 | 15:18:25.21 | 30:35:24.0 | 15.35 | 15.38 | 21.6 | | 23666 | 51 |
| 113 | 15:18:44.13 | 30:38:04.8 | 15.41 | 15.36 | 21.6 | | 24285 | 35 |
| 21 | 15:20:32.49 | 30:04:23.2 | 15.44 | 15.43 | 21.6 | | 22747 | 82 |
| 22 | 15:20:31.56 | 30:10:01.6 | 15.58 | 15.60 | 21.6 | G + | 32789 | 49 |
| 68 | 15:19:36.00 | 30:16:39.7 | 15.64 | 15.57 | 21.6 | | 22185 | 62 |
| | | | | Field 1524 + 2805 | | | | |
| 173 | 15:22:18.47 | 27:44:08.0 | 15.07 | 15.21 | 21.6 | | 20415 | 52 |
| 14 | 15:25:08.23 | 27:46:36.0 | 15.08 | 15.13 | 21.6 | G + | 22374 | 36 |
| 160 | 15:22:26.93 | 27:53:43.4 | 15.44 | 15.44 | 21.6 | | 20875 | 71 |
| 158 | 15:22:28.85 | 27:48:34.4 | 15.49 | 15.46 | 21.6 | | 20821 | 75 |
| 136 | 15:22:45.78 | 27:56:14.0 | 15.57 | 15.57 | 21.6 | | 21137 | 38 |
| | | | | Abell 2079 | | | | |
| 128 | 15:25:40.46 | 29:06:05.3 | 13.37 | * | 21.6 | G + | 19547 | 38 |
| 176 | 15:25:10.12 | 28:57:42.8 | 14.12 | * | 21.6 | | 10227 | 39 |
| 113 | 15:25:48.35 | 29:10:51.4 | 14.12 | * | 21.6 | | 20629 | 37 |
| 203 | 15:24:53.59 | 29:01:33.9 | 14.18 | * | 21.6 | G + | 10406 | 65 |
| 45 | 15:26:27.94 | 29:10:26.8 | 14.22 | * | 21.6 | | 19863 | 46 |
| 129 | 15:25:39.66 | 29:05:28.1 | 14.26 | * | 21.6 | G + | 19541 | 35 |
| 151 | 15:25:22.86 | 28:52:23.8 | 14.61 | 14.72 | 21.6 | | 19330 | 36 |
| 178 | 15:25:07.54 | 28:47:19.9 | 14.68 | 14.82 | 21.6 | | 19349 | 48 |
| 211 | 15:24:41.07 | 29:13:52.2 | 14.70 | 14.81 | 21.6 | | 20221 | 80 |
| 74 | 15:26:05.23 | 29:00:51.6 | 14.77 | 14.86 | 21.6 | | 19989 | 43 |
| 181 | 15:25:07.55 | 28:53:53.7 | 14.90 | 14.95 | 21.6 | | 20846 | 45 |
| 164 | 15:25:19.12 | 29:01:21.6 | 14.93 | 14.96 | 21.6 | | 19529 | 38 |
| 229 | 15:24:11.03 | 28:50:40.5 | 15.02 | 15.06 | 21.6 | | 20179 | 48 |
| 179 | 15:25:08.49 | 28:56:20.0 | 15.04 | 15.06 | 21.6 | | 18600 | 38 |
| 31 | 15:26:39.76 | 29:16:20.0 | 15.05 | 15.15 | 21.6 | | 19473 | 32 |
| 88 | 15:25:57.84 | 29:06:58.3 | 15.05 | 15.05 | 21.6 | | 20196 | 40 |
| 35 | 15:26:36.68 | 29:14:45.2 | 15.08 | 15.08 | 21.6 | | 19440 | 36 |
| 2 | 15:27:06.72 | 29:12:09.2 | 15.12 | 15.10 | 21.6 | | 24990 | 36 |
| 71 | 15:26:05.31 | 28:49:54.1 | 15.15 | * | 21.6 | G + | 18552 | 40 |
| 83 | 15:26:01.57 | 29:10:59.5 | 15.18 | 15.17 | 21.6 | | 18419 | 46 |
| 101 | 15:25:54.83 | 29:21:59.2 | 15.22 | 15.18 | 21.6 | G + | 19918 | 51 |
| 23 | 15:26:46.45 | 29:13:42.0 | 15.27 | 15.24 | 21.6 | | 20986 | 34 |
| 134 | 15:25:37.37 | 29:04:54.6 | 15.29 | 15.24 | 21.6 | | 19856 | 31 |
| 193 | 15:25:03.98 | 29:20:06.1 | 15.31 | 15.30 | 21.6 | | 19973 | 46 |
| 145 | 15:25:28.63 | 29:01:29.8 | 15.32 | 15.27 | 21.6 | | 9775 | 38 |
| 46 | 15:26:27.63 | 29:08:08.4 | 15.36 | 15.32 | 21.6 | | 19070 | 64 |
| 210 | 15:24:39.93 | 29:00:23.0 | 15.46 | 15.39 | 21.6 | | 22249 | 41 |
| 56 | 15:26:21.36 | 29:13:43.7 | 15.56 | 15.50 | 21.6 | | 25633 | 42 |
| 240 | 15:23:59.49 | 29:54:19.3 | 15.58 | 15.53 | 21.6 | | 20215 | 48 |
| 60 | 15:26:21.76 | 29:26:22.1 | 15.63 | 15.66 | 21.6 | G + | 19052 | 38 |
| 167 | 15:25:19.38 | 29:21:51.7 | 15.64 | 15.57 | 21.6 | | 20795 | 35 |
| 149 | 15:25:26.44 | 29:03:07.3 | 15.66 | 15.57 | 21.6 | | 19343 | 45 |
| | | | | Abell 2089 | | | | |
| 121 | 15:30:44.49 | 28:12:26.0 | 14.50 | * | 21.6 | G + | 21960 | 43 |
| 122 | 15:30:41.36 | 28:32:02.4 | 14.70 | 14.85 | 21.6 | | 21701 | 56 |
| 287 | 15:29:17.40 | 28:15:39.9 | 15.14 | 15.36 | 21.6 | | 22209 | 52 |
| 180 | 15:30:17.70 | 28:07:22.9 | 15.39 | 15.48 | 21.6 | | 21814 | 42 |
| 108 | 15:30:53.73 | 28:03:44.6 | 15.43 | 15.32 | 21.6 | G + | 21492 | 36 |
| 14 | 15:32:07.34 | 28:13:26.6 | 15.53 | 15.64 | 21.6 | | 22314 | 33 |
| 205 | 15:30:05.28 | 28:16:16.2 | 15.60 | 15.66 | 21.6 | | 22495 | 48 |
| 43 | 15:31:36.48 | 28:18:43.6 | 15.62 | 15.60 | 21.6 | G + | 5607 | 38 |
| 300 | 15:29:11.49 | 28:05:59.5 | 15.63 | 15.64 | 21.6 | | 22914 | 48 |
| | | | | Abell 2092 | | | | |
| 185 | 15:31:11.46 | 31:28:22.7 | 14.29 | * | 21.6 | | 16170 | 29 |
| 61 | 15:32:38.58 | 31:45:42.8 | 14.59 | * | 21.6 | | 19663 | 43 |
| 16 | 15:33:32.46 | 31:41:10.8 | 14.84 | 15.08 | 21.6 | | 16084 | 42 |
| 181 | 15:31:13.77 | 31:18:43.6 | 14.86 | * | 21.6 | | 20175 | 45 |
| 172 | 15:31:18.50 | 31:22:46.4 | 15.41 | 15.47 | 21.6 | | 20166 | 35 |
| 165 | 15:31:22.16 | 31:20:48.8 | 15.53 | 15.54 | 21.6 | | 18927 | 34 |
| 62 | 15:32:37.41 | 31:52:03.1 | 15.54 | 15.61 | 21.6 | | 32065 | 44 |
| 118 | 15:31:45.29 | 31:50:34.4 | 15.63 | 15.65 | 21.6 | G + | 26995 | 33 |

Note to TABLE I

Asterisk indicates object with companion within the aperture.

© American Astronomical Society • Provided by the NASA Astrophysics Data System

1986AJ.....92.1238P



TABLE II. Data for filled survey of the Cor Bor region.

| ID | R.A. (1950) | Dec. | *B* mag | Vel. | Err. | Vel. Source |
|---|---|---|---|---|---|---|
| NGC 5958 | 15:32:42.00 | 28:50:0.0 | 13.20 | 2021 | 36 | E |
| NGC 5961 | 15:33:12.00 | 31:01:0.0 | 14.00 | 1828 | 20 | D |
| NGC 5974 | 15:37:00.00 | 31:55:0.0 | 14.30 | 2007 | 35 | E |
| 1515 + 3052 | 15:15:54.00 | 30:52:0.0 | 14.70 | 9230 | 35 | A |
| 1520 + 2957 | 15:20:42.00 | 29:57:0.0 | 14.90 | 6850 | 32 | A |
| IC 4569 | 15:38:42.00 | 28:28:0.0 | 15.00 | 9821 | 19 | A |
| IC 4572 | 15:39:48.00 | 28:18:0.0 | 15.00 | 9919 | 26 | A |
| 1533 + 3058 | 15:33:18.00 | 30:58:0.0 | 15.10 | 9352 | 28 | A |
| 1527 + 3039 | 15:27:42.00 | 30:39:0.0 | 15.10 | 10454 | | F |
| 1541 + 2835 | 15:41:42.00 | 28:35:0.0 | 15.10 | 10051 | 30 | A |
| IC 4570 | 15:39:12.00 | 28:24:0.0 | 15.10 | 9637 | 31 | A |
| 1517 + 3133 | 15:17:48.00 | 31:33:0.0 | 15.20 | 9405 | 38 | A |
| 1534 + 3117 | 15:34:24.00 | 31:17:0.0 | 15.20 | 14701 | 44 | A |
| 1534 + 3051 | 15:34:18.00 | 30:51:0.0 | 15.20 | 1800 | | B |
| 1524 + 2653 | 15:24:54.00 | 26:53:0.0 | 15.20 | 10191 | 27 | A |
| 1539 + 2809 | 15:39:18.00 | 28:09:00 | 15.20 | 9641 | 23 | A |
| 1533 + 2730 | 15:33:06.00 | 27:30:0.0 | 15.20 | 9706 | 37 | A |
| 1523 + 2946 | 15:23:36.00 | 29:46:0.0 | 15.20 | 16693 | 34 | A |
| 1519 + 2844 | 15:19:12.00 | 28:44:0.0 | 15.30 | 9437 | 33 | A |
| IC 4581 | 15:41:54.00 | 28:26:0.0 | 15.30 | 9973 | 33 | A |
| 1528 + 2716 | 15:28:12.00 | 27:16:0.0 | 15.30 | 9794 | 44 | A |
| 1512 + 2647 | 15:12:24.00 | 26:47:0.0 | 15.30 | 9649 | 25 | A |
| 1538 + 2831A | 15:38:24.00 | 28:31:0.0 | 15.30 | 9805 | 20 | A |
| IC 4568 | 15:38:00.00 | 28:19:0.0 | 15.30 | 9376 | 27 | A |
| 1542 + 2737 | 15:42:00.00 | 27:37:0.0 | 15.40 | 9624 | 32 | A |
| 1523 + 2644A | 15:23:24.00 | 26:44:0.0 | 15.40 | 10250 | 29 | A |
| IC 4580 | 15:41:06.00 | 28:31:0.0 | 15.40 | 9567 | 24 | A |
| 1528 + 2718 | 15:28:06.00 | 27:18:0.0 | 15.40 | 9700 | 36 | A |
| 1534 + 2729 | 15:34:06.00 | 27:29:0.0 | 15.40 | 9866 | 29 | A |
| 1522 + 3027 | 15:22:18.00 | 30:27:0.0 | 15.40 | 9357 | 37 | A |
| 1541 + 2841 | 15:41:36.00 | 28:41:0.0 | 15.50 | 9832 | 29 | A |
| 1536 + 2935 | 15:36:42.00 | 29:35:0.0 | 15.50 | 9792 | 39 | A |
| 1532 + 3114 | 15:32:42.00 | 31:14:0.0 | 15.50 | 1868 | 25 | C |
| 1531 + 2730 | 15:31:54.00 | 27:30:0.0 | 15.50 | 10223 | 31 | A |
| 1525 + 2824 | 15:25:36.00 | 28:24:0.0 | 15.50 | 10303 | 33 | A |
| 1520 + 2635 | 15:20:00.00 | 26:35:0.0 | 15.50 | 13541 | 27 | A |
| 1519 + 3050 | 15:19:00.00 | 30:50:0.0 | 15.50 | 9239 | 20 | A |

Velocity Sources for Table II

A—Huchra, J., this paper.
B—Denisyuk, E., Lipovetsky, V., Afanasev, V. (1976). Astrofizica **12**, 667.
C—Bothun, G., Beers, T., Mould, J., and Huchra, J. (1985). Astron. J. **90**, 2487.
D—Romanishin, W. (1980). Private communication.
E—Huchra, J., Davis, M., Latham, D., and Tonry, J. (1982). Astrophys. J. Suppl. **52**, 89.
F—Palumbo, G., Tanzella-Nitti, G., and Vettolani, G. (1983). *Catalogue of Radial Velocities of Galaxies* (Gordon and Breach, New York).

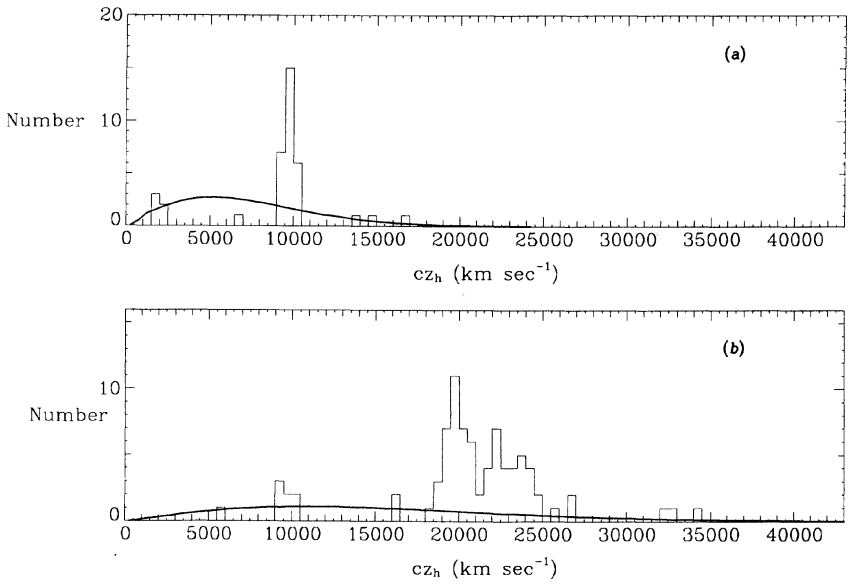


FIG. 4 (a) Radial-velocity histogram for the filled survey of Cor Bor to $m_{B(0)} = 15.5$. The smooth curve is the expected distribution for a uniform universe. (b) Radial-velocity histogram for the unfilled survey of Cor Bor to $m_R = 15.7$.

© American Astronomical Society • Provided by the NASA Astrophysics Data System

1986AJ.....92.1238P



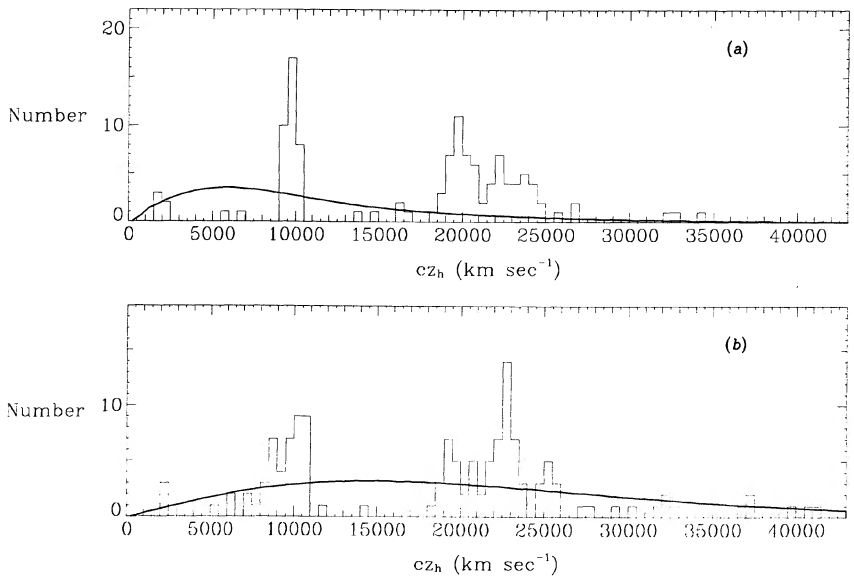


FIG. 5 (a) Radial-velocity histogram for the combined magnitude-limited survey of Cor Bor. The smooth curve is the expected distribution for a uniform universe. (b) Radial-velocity histogram for the Boötes survey fields NP 5, NP 7, and NP 8.

in the region. Figure 5(a) shows the histogram of 120 velocities in the combined $B(0)$ and $R$ magnitude-limited samples. The smooth curve is the predicted distribution for a complete sample with $m_{B(0)} \leqslant 15.5$ over 39.2 square degrees and $m_R \leqslant 15.7$ over 3.4 square degrees in a uniform universe.

The radial-velocity distributions for the KOSS (1981) survey fields NP 5, NP 7, and NP 8 near Boötes are reproduced in Fig. 5(b). These three fields are widely separated on the sky (see Fig. 2) and lie on the perimeter of the more extensive survey of Boötes (KOSS 1986). The fields cover 5.9 square degrees and contain 133 galaxies. The expected distribution for the Boötes survey was computed using Eq. (2) with the CfA luminosity-function parameters.

### *b) Results*

The large inhomogeneities in the radial-velocity histograms for the Cor Bor and Boötes surveys are strikingly similar. Here we consider each of the structures in the Cor Bor region in detail.

The underdense region ("void") centered at 6500 km s$^{-1}$, comparable with the void in Boötes, and the thin, overdense shell at 9500 km s$^{-1}$ were originally detected in the extension of the CfA redshift survey (LGH). In the full CfA survey extension there are a few galaxies which form a very low-density structure inside the void. This structure includes galaxies just to the east and west of the surveys discussed here (LGH 1986). Even including these galaxies, the density in the void is only 20% of the expected mean derived from Eq. (2).

The unfilled $R$ survey, which reaches $\sim 1.7$ mag fainter than the filled survey, places tighter constraints on the distribution of fainter galaxies inside the void at 6500 km s$^{-1}$. Galaxies with $M \lesssim M^* + 2.5[(L/L^*) \gtrsim 0.1]$ should be detected in this region. We find one galaxy when we expect eight. In the filled survey, there is also one galaxy in this redshift range: we expect 28. The two surveys and the full CfA survey extension give consistent estimates of the underdensity in the region.

About 30% of the galaxies in the combined survey lie in the interval 9000–10 500 km s$^{-1}$, implying a density contrast $n/\bar{n} \approx 4$. The cone diagram for this survey [Fig. 6(a)] shows this thin, shell-like structure. The structure remains apparent in Fig. 6(b), a cone diagram for all 231 galaxies in the region which have measured redshifts. These data include the published results of Humason *et al.* (1956), Denisyuk *et al.* (1976), Spinrad (1977), Thuan and Seitzer (1979), Gioia *et al.* (1982), Huchra *et al.* (1982), Palumbo *et al.* (1983), Bothun *et al.* (1985), and data soon to be published by Postman, Geller, and Huchra (1986). A detailed velocity reference table will be presented at that time. Light circles denote galaxies with $m_{B(0)} \leqslant 15.5$. Seven of the 83 galaxies in the unfilled survey are in the shell (for a density contrast of $\sim 4$ we expect 12 galaxies in this structure). Although the feature stands out readily in velocity space, it has a surface density of only $\sim 1$ galaxy deg$^{-2}$ for $m_{B(0)} \leqslant 15.5$.

Within the limits of our surveys, the total width of the shell, $\sim 1000$ km s$^{-1}$, does not change significantly as a function of luminosity. Figure 7 shows the velocity histogram for galaxies in the shell as a function of $B(0)$ magnitude for the combined survey. $R$ magnitudes are converted to $B(0)$ magnitudes assuming $[B(0) - R] = 1.5$. The mean and standard deviation of the velocities for the 17 galaxies brighter than $m_{B(0)} = 15.3$ are $9732 \pm 76$ km s$^{-1}$ and $300^{+72}_{-44}$ km s$^{-1}$, respectively. For the 18 galaxies fainter than $m_{B(0)} = 15.3$ the mean velocity and standard deviation are $9762 \pm 88$ km s$^{-1}$ and $361^{+83}_{-49}$ km s$^{-1}$, respectively. The faintest galaxies in the shell are near the limit of the $R$ survey with $L/L^* = 0.20$.

In the range 11 000–17 000 km s$^{-1}$ there are five galaxies observed in the combined survey; 20 are expected in a homogeneous universe. This density contrast is comparable with that for the void in Boötes ($n/\bar{n} \approx 0.25$). Galaxies with $M \lesssim M^* + 1(L/L^* \gtrsim 0.4)$ should be detected in this velocity range. It is hard to evaluate the significance of this void because (1) the actual survey volume is small and (2) although the redshift distributions in the five deep probes are all nearly the same, four of the five probes cover the cores of rich clusters which were known *a priori* to be at similar redshift. Nonetheless, the large separation of the probes ($\sim 15h^{-1}$ Mpc at 15 000 km s$^{-1}$) combined with the similarity of their velocity histograms over the entire redshift

© American Astronomical Society • Provided by the NASA Astrophysics Data System

1986AJ.....92.1238P



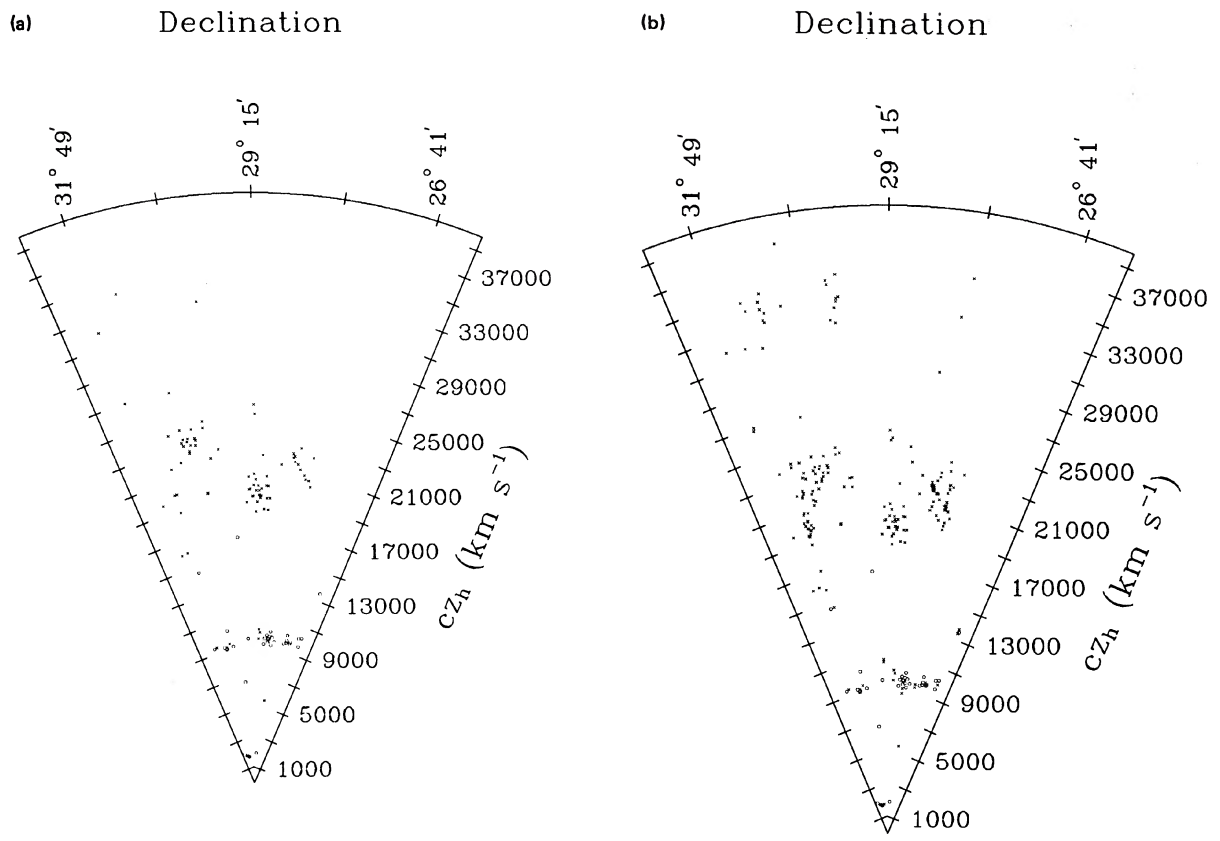


FIG. 6. (a) Cone diagram ($\delta$ vs redshift) showing the 120 galaxies in the combined magnitude-limited survey of Cor Bor. The cone diagram is expanded to show the data clearly. Light circles represent galaxies with $m_{B(0)} \leqslant 15.5$. (b) Cone diagram showing all galaxies with measured redshifts in the Cor Bor region. These galaxies do not comprise a complete magnitude-limited sample.

range indicates the presence of a void. A larger filled survey (Geller *et al.* 1987a), which covers a $\sim 7° \times 1°$ strip centered at $\delta = +29.5°$ and which is complete to $m_R \approx 15.5$, contains only five galaxies in this redshift range. There are 18 expected. Taken together, these surveys confirm that there is a real void in this velocity range.

Remarkably, the void in Boötes, which is centered about 18° to the northwest of the Cor Bor survey, extends over a similar redshift range. KOSS (1986) estimate that the largest empty sphere which can fit inside the Boötes void has a radius of $\sim 32h^{-1}$ Mpc. If these voids are similar in nature to the voids detected in the CfA survey extension, then the galaxy-rich boundaries surrounding them are very thin (thickness $\lesssim 5h^{-1}$ Mpc). Consequently, unfilled surveys can easily miss detecting void boundaries lying parallel to the line of sight. The Cor Bor void centered at 13 500 km s$^{-1}$ is prob-

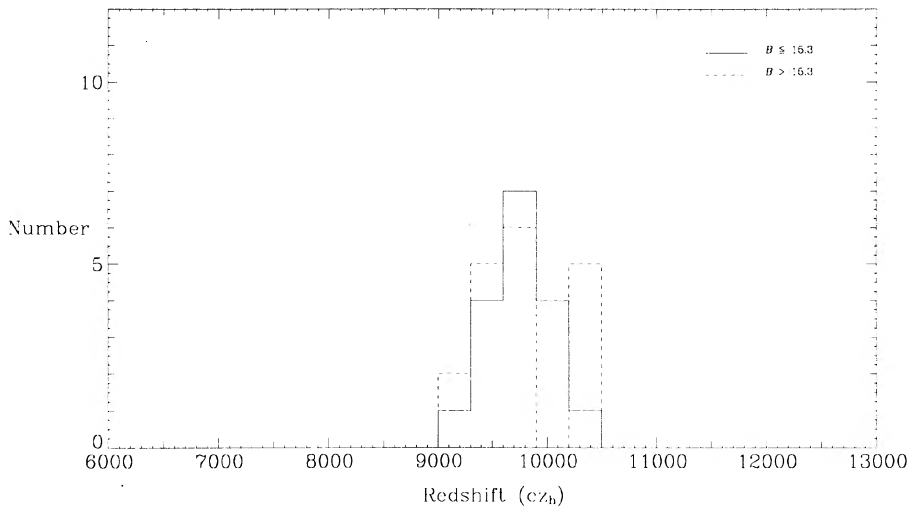


FIG. 7. Radial-velocity distribution for Cor Bor galaxies in the shell at 9500 km s$^{-1}$ as a function of $B(0)$ luminosity. The solid histogram shows the distribution for galaxies with $m_{B(0)} \leqslant 15.3$. The dashed histogram shows the distribution for galaxies with $m_{B(0)} > 15.3$.

© American Astronomical Society • Provided by the NASA Astrophysics Data System

1986AJ.....92.1238P



ably a separate structure and not an extension of the Boötes void. The angular spread of the Cor Bor survey fields places a lower limit of $\sim 13h^{-1}$ Mpc on the radius of this newly detected void, a volume of $\sim 9000h^{-3}$ Mpc$^3$. The radius may be as large as $25h^{-1}$ Mpc if the extent of the void in redshift space is a reliable indicator of scale. The topology and connectiveness of the Boötes and Cor Bor voids are subjects still to be explored.

Out of the entire sample of 231 redshifts [Fig. 6(b)], there are ten galaxies in the range 11 000–17 000 km s$^{-1}$. The positions of these galaxies are close to the positions of galaxies in the magnitude-limited surveys. The spectra of these ten galaxies were examined for emission-line features. Only three of the ten galaxies show even moderate to weak H$\alpha$ emission.

The Cor Bor supercluster is the cause of the large density enhancement in the 18 000–25 000 km s$^{-1}$ range. This feature is broadened by the internal velocity dispersions of A2061, A2079, A2089, and A2092. The density contrast in this redshift range is $\sim 7$. The Cor Bor supercluster is embedded in a shell which extends at least to the southeastern edge of the Boötes region. The five galaxies in the field region 1524 + 2805 all lie at a redshift of $\sim 21\,000$ km s$^{-1}$.

The similarity between the galaxy distribution in the Cor Bor survey and the distribution in the KOSS (1981) Boötes survey (which does not contain a supercluster) suggest that large voids are common, in agreement with the CfA survey-extension results. The similarity between the two distributions also suggests that large voids have characteristic radii in the range $15–30h^{-1}$ Mpc. In a universe populated with voids of some characteristic diameter surrounded by thin shells of galaxies, one expects similar radial-velocity histograms for fields which probe to a depth two or three times the typical void diameter and which are separated by as much as three typical void diameters (de Lapparent and Geller 1986).

## V. CONCLUSIONS

Deep, unfilled surveys of the distribution of galaxies are an important tool for detecting and examining the largest structures. Combined with shallower filled surveys they provide constraints on the distribution of galaxies as a function of luminosity.

The failure to find more than one faint galaxy in the void centered at 6500 km s$^{-1}$ and the invariance of the width of the shell at 9500 km s$^{-1}$ suggests that the topology of the galaxy distribution in redshift space is insensitive to luminosity for $M_{B(0)} \lesssim -17.4$. The distribution of galaxies around the small void in front of the Coma cluster (LGH 1986) also indicates luminosity independence in this magnitude range. The constraints on the relative distribution of high and low-surface-brightness galaxies, however, remain poor (Bothun *et al.* 1986).

The surveys of Boötes and of Cor Bor indicate that at depths between 100 and $250h^{-1}$ Mpc the galaxy distribution has characteristics similar to those revealed by the CfA survey extension (LGH 1986). In particular, large voids are ubiquitous. The galaxy number density contrast $n/\bar{n}$ within the voids is typically $\sim 0.2–0.3$. The void we detect in the 11 000–17 000 km s$^{-1}$ range is confirmed by a more extensive filled survey. The remarkable similarity between the galaxy distribution in the Cor Bor region and in Boötes can be explained in a bubble-like geometry where large voids have radii between 15 and $30h^{-1}$ Mpc. The structures which extend across the sky at 10 000 km s$^{-1}$ and at 21 000 km s$^{-1}$ probably are the surfaces of many adjacent bubbles.

This survey and others (Gregory and Thomson 1978; Jôeveer, Einasto, and Tago 1978; Gregory, Thomson, and Tifft 1981; Bahcall and Soneira 1982; Giovanelli, Haynes, and Chincarini 1986) suggest that there is a physical relationship between the clusters, superclusters, and voids. LGH suggest that clusters occur preferentially in the interstices between bubbles (the Coma cluster is an example). They are connected by the surfaces surrounding the voids. In this model, superclusters are always associated with voids and their properties are dictated by the geometry of the associated large-scale structure.

Our maps of large-scale structure cover regions far too small to place stringent constraints on the relationship between superclusters and voids and for reliable limits to be set on the largest structures. To date, every survey which probes a sufficiently large volume contains inhomogeneities on $25–50h^{-1}$ Mpc scales. We have recently completed a whole-sky, magnitude-limited survey of Abell clusters out to $z \sim 0.1$ (Geller *et al.* 1987b). A direct comparison between the galaxy and cluster distributions should eventually clarify the relationship between clusters, superclusters, and large voids.

We are grateful to the staffs of the Multiple Mirror Telescope and the Whipple Observatory for their assistance with the observations. We also thank the staffs of the Kitt Peak National Observatory and Yale University for the use of their PDS machines. We especiallly thank Michael Kurtz for valuable advice regarding the analysis of the PDS images, and R. Schild and S. Kent for their assistance with the reductions of the CCD data. R. Kirshner has kept us informed about the latest results on the nature of the void in Boötes and provided us with Fig. 2. We also thank the referee, A. Oemler, for useful comments on the manuscript. This research is supported by NASA grant NAGW-201. M. Postman is supported by a NASA fellowship.

## REFERENCES

Aaronson, M., Huchra, J., Mould, J., Schechter, P., and Tully, J. (1982). Astrophys. J. **258**, 64.
Abell, G. O. (1958). Astrophys. J. Suppl. **3**, 211.
Bahcall, N., and Soneira, R. (1982). Astrophys. J. **262**, 419.
Binggeli, B. (1982). Astron. Astrophys. **107**, 338.
Bothun, G., Beers, T., Mould, J., and Huchra, J. (1985). Astron. J. **90**, 2487.
Bothun, G., Beers, T., Mould, J., and Huchra, J. (1986). Preprint.
Davis, M., and Huchra, J. (1982). Astrophys. J. **254**, 437.
de Lapparent, V., and Geller, M. (1986). In preparation.
de Lapparent, V., Geller, M., and Huchra, J. (1986). Astrophys. J. Lett. **302**, L1 (LGH).
Denisyuk, E., Lipovetsky, V., and Afanasev, V. (1976). Astrofizica **12**, 667.
Einasto, J., Jôeveer, M., and Saar, E. (1980). Mon. Not. R. Astron. Soc. **193**, 353.
Faber, S. (1986). Heineman Prize Lecture at 167th AAS Meeting, Houston, TX.
Geller, M., Huchra, J., and Kurtz, M. (1987a). In preparation.

© American Astronomical Society • Provided by the NASA Astrophysics Data System

1986AJ.....92.1238P



Geller, M., Huchra, J., and Postman, M. (1987b). In preparation.
Gioia, I., Geller, M., Huchra, J., Maccacaro, T., Steiner, J., and Stocke, J. (1982). Astrophys. J. Lett. **255**, L17.
Giovanelli, R., Haynes, M., and Chincarini, G. (1986). Astrophys. J. **300**, 77.
Gregory, S. A., and Thomson, L. A. (1978). Astrophys. J. **222**, 784.
Gregory, S. A., Thomson, L. A., and Tifft, W. G. (1981). Astrophys. J. **243**, 411.
Huchra, J., Davis, M., Latham, D., and Tonry, J. (1982). Astrophys. J. Suppl. **52**, 89.
Humason, M., Mayall, N. U., and Sandage, A. R. (1956). Astron. J. **61**, 97.
Jôeveer, M., Einasto, J., and Tago, E. (1978). Mon. Not. R. Astron. Soc. **185**, 357.
Kirshner, R., Oemler, A., Schechter, P., and Shectman, S. (1981). Astrophys. J. Lett. **248**, L57 (KOSS 1981).
Kirshner, R., Oemler, A., Schechter, P., and Shectman, S. (1986). Astrophys. J. (submitted) (KOSS 1986).
Kron, G., White, H., and Gascoigne, S. (1953). Astrophys. J. **118**, 502.
Kurtz, M., Huchra, J., Beers, T., Geller, M., Gioia, I., Maccacaro, T., Schild, R., and Stauffer, J. (1985). Astron. J. **90**, 1665.
Palumbo, G., Tanzella-Nitti, G., and Vettolani, G. (1983). *Catalogue of Radial Velocities of Galaxies* (Gordon and Breach, New York).
Postman, M., Geller, M., and Huchra, J. (1986). In preparation.
Sargent, W., and Turner, E. (1977). Astrophys. J. Lett. **212**, L3.
Schechter, P. (1976). Astrophys. J. **203**, 297.
Schild, R. (1984). Publ. Astron. Soc. Pac. **95**, 1021.
Schild, R., and Kent, S. (1981). SPIE J. **290**, 186.
Spinrad, H. (1977). Publ. Astron. Soc. Pac. **89**, 116.
Tarenghi, M., Chincarini, G., Rood, H. J., and Thomson, L. A. (1980). Astrophys. J. **235**, 724.
Thuan, T., and Seitzer, P. (1979). Astrophys. J. **231**, 327.
Valdes, F. (1982). Proc. SPIE **331**, 465.

© American Astronomical Society • Provided by the NASA Astrophysics Data System